Materials Horizons

Full-colour Jabuticaba-like nanostructures via multiplex and orthogonal self-assembly of protein conjugated quantum dots with engineered biofilms

Journal:	*Materials Horizons*
Manuscript ID	MH-COM-10-2022-001231.R1
Article Type:	Communication
Date Submitted by the Author:	27-Jan-2023
Complete List of Authors:	Deng, Zhengtao; Nanjing University, College of Engineering and Applied Sciences Chen, Allen; MIT Zakeri, Bijan; MIT Zhong, Chao; ShanghaiTech University, School of Physical Science and Technology; MIT, Lu, Timothy ; MIT, Biological Engineering and Electrical Engineering and Computer Science

New Concept

The integration of inorganic components with living cells is of broad interest for expanding the functionality of materials for a wide range of applications. While DNA-directed assembly of inorganic materials offers high specificity and control, it is difficult to integrate this strategy with living cells as there are few cell-produced extracellular scaffolds for DNA. Furthermore, it is challenging to produce DNA-based materials in bulk due to high costs. Protein-based or phage-based scaffolds are in principle suitable for the assembly of inorganic materials, but currently do not offer sufficient specificity for the assembly of multi-component materials, as they have largely relied on metal-peptide coordination chemistries. To tackle these challenges, we engineered cellular consortia composed of multiple distinct cell populations to manufacture scaffold subunits with defined, orthogonal specificities. Specifically, we genetically engineered *Escherichia coli*-produced amyloid fibrils to display multiple orthogonal isopeptide bond-forming peptides (e.g., SpyTag, IsopepTagN and IsopepTagC) that bind specifically to their cognate protein partners. This enabled the programmable, scalable, multiplexed, and highly specific coupling of inorganic materials to extracellular amyloid scaffolds. We applied this platform to assemble quantum dots (QDs) in to full-colour Jabuticaba-like nanostructures. Moreover, we showed that this platform is readily scaled-up at low cost due to the ease of growing large bacterial populations. We envision that genetically engineering living cell-produced scaffolds for the scalable, multiplexed, and specific self-organization of nanomaterials will enable the creation of new hierarchical architectures and functional devices with integrated living and non-living components.

COMMUNICATION

Full-colour Jabuticaba-like nanostructures via multiplex and orthogonal self-assembly of protein conjugated quantum dots with engineered biofilms

Received 00th January 20xx,
Accepted 00th January 20xx

DOI: 10.1039/x0xx00000x

Zhengtao Deng[a,b*], Allen Y. Chen[a], Bijan Zakeri[a], Chao Zhong[a,c], Timothy K. Lu[a*]

The integration of inorganic components with bacterial biofilms is of great significance for expanding the functionality of artificial biological materials. However, so far, the complexities and functionalities of biofilm-based scaffolds assembled by metal-peptide coordination chemistries are still limited. Here, we present a platform for the multiplexed and specific coupling of recombinant protein-functionalized fluorescent red-green-blue (RGB) quantum dots (QDs) with engineered biofilms to form Jabuticaba-like nanostructures. Full color living Jabuticaba-like nanostructures have been achieved through the interaction of extracellular peptides that are fabricated by biofilms with the proteins that are modified the surface of the RGB QDs through orthogonal SpyTag-SpyCatcher, IsopeptagN-PilinN, and IsopeptagC-PilinC pairs. We envision that living cell populations will enable the multiplexable, scalable and bottom-up assembly of versatile materials that integrate both abiotic and biotic components into multifunctional systems.

The assimilation of inorganic components with living cells in a programmable manner is of broad interest for expanding the functionality of new artificial materials [1-10]. Nature has provided much inspiration for the bottom-up fabrication of complex hierarchical architectures [11-13]. Moreover, previous efforts have described the development of various bio-inspired scaffolds for assembling functionalized inorganic nanomaterials [14-27]. For example, DNA origami enables precise self-assembly of DNA-oligonucleotide-functionalized AuNPs or QDs through highly specific Watson-Crick base-pairing interactions, but it can be challenging to integrate this strategy with living cells and to scale DNA-based materials due to high cost [15-20]. Previously, protein-based scaffolds have been used to biomineralize single-component inorganic nanoparticles via metal-peptide coordination chemistries [21-23]. Leveraging living cells for materials synthesis and patterning can provide complementary capabilities to these non-living templated assembly strategies, such as scalable self-organization of larger-scale structures [21-25]. Recently, we showed that orthogonal control over materials production with synthetic gene circuits in living bacteria enables temporal and multi-scale spatial control over materials assembly [28]. Bacterial biofilms have been used to template the assembly of single inorganic materials for a specific system [28, 29]. However, the complexities and functionalities are still limited.

Here, we demonstrate that genetically engineered *Escherichia coli* biofilms can achieve large-scale organization of a wide array of functional protein-conjugated fluorescent RGB QDs into full color living Jabuticaba-like nanostructures with high complexity and specificity, as shown in Scheme **1**.

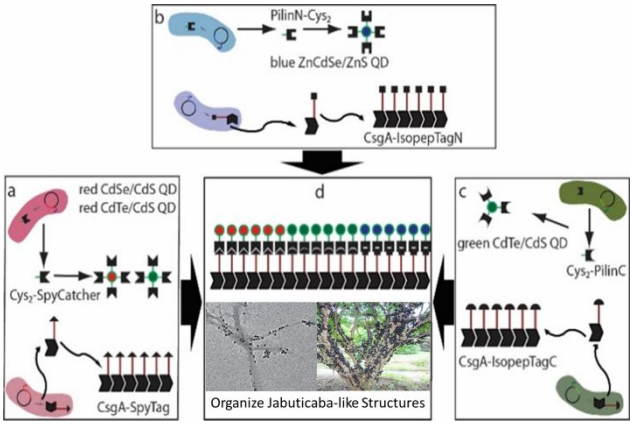

Scheme 1. Schematic illustrating the organization of protein-conjugated RGB QDs with living cells *via* **a**, SpyTag-SpyCatcher; **b**, IsopeptagN-PilinN; **c**, IsopeptagC-PilinC interaction pairs. (**d**) The orthogonal isopeptide bond-forming chemistries enable the formation of full color QD Jabuticaba-like structures.

[a.] *Research Laboratory of Electronics, Department of Electrical Engineering & Computer Science, Department of Biological Engineering, MIT Synthetic Biology Center, Harvard-MIT Health Sciences and Technology, Massachusetts Institute of Technology, Cambridge, MA 02139, USA. Email: timlu@mit.edu (TKL)*
[b.] *College of Engineering and Applied Sciences, State Key Laboratory of Analytical Chemistry for Life Science, National Laboratory of Microstructures, Nanjing University, Nanjing, Jiangsu, 210023, P. R. China. Email: dengz@nju.edu.cn (Z.D.)*
[c.] *Materials Synthetic Biology Center, Shenzhen Institute of Synthetic Biology, Shenzhen Institutes of Advanced Technology, Chinese Academy of Sciences, Shenzhen 518055, P. R. China.*
Electronic Supplementary Information (ESI) available: Experimental and characterization details; TEM images; PL spectra; photographs; EDS spectra; See DOI: 10.1039/x0xx00000x

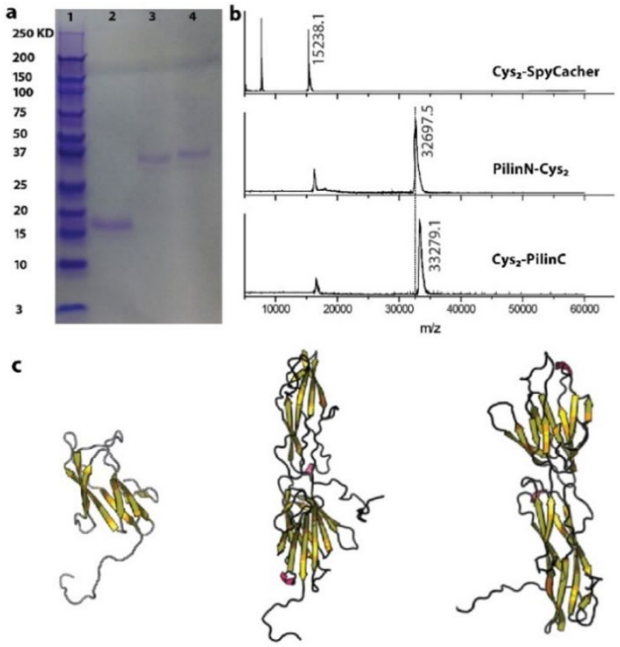

Fig. 1 (**a**, **b**) Coomassie-stained SDS-PAGE gels and the matrix-assisted laser desorption ionization (MALDI)-time-of-flight (TOF) spectra analysis of the purified recombinant proteins. In **a**, Lane 1 is the standard protein ladder, while Lanes 2, 3, and 4 represent the recombinant Cys_2-SpyCatcher, PilinN-Cys_2 and Cys_2-PilinC, respectively. (c) from left to right shows the structural simulations for Cys_2-SpyCatcher, PilinN-Cys_2 and Cys_2-PilinC, respectively. Simulations were performed via RaptorX[30].

This organization is mediated by cell-synthesized amyloid fibrils known as curli [28, 29], which are expressed under the artificial control of chemical inducers. This platform is readily scaled-up at low cost due to the ease of growing large bacterial populations. Amyloids constitute a natural self-assembled protein material comparable in specific stiffness to spider silk and steel [31-34]. Amyloid fibrils are on the order of microns in length and three to tens of nanometers in width, and are stabilized by hydrogen bonds and hydrophobic interactions [35, 36]. We genetically engineered *E. coli* to express self-assembling curli amyloid subunits, CsgA, under tight transcriptional and translational regulation (Methods, Supplementary Table S1-S3). CsgA is engineered to display orthogonal peptide tags, including SpyTag, IsopeptagN, and IsopeptagC. We also functionalized QDs with the recombinant proteins Cys_2-SpyCatcher, PilinN-Cys_2 and Cys_2-PilinC, which bind specifically to the peptide tags and form covalent bonds.

The living biomanufacturing platform leverages the advantages of orthogonal isopeptide bond-forming chemistries to mediate specific QD-curli interactions. For example, SpyTag-SpyCatcher chemistry involves a genetically encodable, specific, and highly reactive peptide-protein pair engineered by splitting the autocatalytic intramolecular isopeptide bond in the CnaB2 domain from *Streptococcus pyogenes* [37]. Upon simple mixing, SpyTag and SpyCatcher undergo autocatalytic intermolecular isopeptide bond formation between Asp117 on SpyTag and Lys31 on SpyCatcher, resulting in irreversible amide bond formation in minutes within both *in vitro* and *in vivo* environments. IsopeptagN-PilinN and IsopeptagC-PilinC chemistries work in an analogous fashion [38]. Since the reactive units are conveniently introduced by genetic engineering, all these chemistries are excellent platforms for organizing protein-conjugated QDs with cell-synthesized scaffolds.

Genes encoding the designed proteins were appended with N-terminal $(Cys)_2$ and $(His)_7$ tags for (SpyCatcher and PilinC) or a C-terminal $(Cys)_2$ and $(His)_7$ tag for PilinN (Table S1), and then expressed in *E. coli*, followed by protein purification under non-denaturing conditions by nickel-affinity chromatography. As shown in Figure **1a**, Cys_2-SpyCatcher, PilinN-Cys_2 and Cys_2-PilinC migrated as single bands at ~16, ~33 and ~34 kDa, respectively, under SDS-polyacrylamide gel electrophoresis (SDS-PAGE). As shown in Figure **1b,** more accurate molecular weight assessment via matrix-assisted laser desorption ionization (MALDI)-time-of-flight (TOF) revealed 15.24, 32.70, and 33.28 KDa for these proteins, respectively. These results are consistent with the SDS-PAGE results and theoretical data (15.58, 32.90, 33.55 KDa shown in Table S1). We achieved highly pure (>95%) and highly soluble recombinant proteins with optimized yields of 10 mg/L, which was expected after a single round of Ni-NTA purification [37, 38].

We developed a strategy for rapid and robust QD-protein conjugation coordinated with single-step synthesis in aqueous solution (see Methods). Cysteine (Cys) and histidine (His) linkages were genetically encoded in the recombinant Cys_2-SpyCatcher, PilinN-Cys_2 and Cys_2-PilinC proteins. These linkages have high affinity to metals (such as cadmium and zinc) and were directly incorporated into the shell of the QDs during core/shell QD synthesis, thus providing reliable conjugation at a defined attachment domain on the proteins [39]. We show that this synthetic route results in robust QD-protein conjugates that are highly stable and fluorescent and can be used with a wide range of nanomaterials with variable sizes, geometries, compositions, and surface properties.

CdSe/CdS core/shell QD-SpyCatcher conjugates were created by attaching recombinant Cys_2-SpyCatcher proteins to QDs during the CdS shell formation process (Figures **2a-2c**). First, - 6 nm oleic-acid-capped CdSe QDs with a photoluminescence (PL) emission peak at 650 nm (Figures **2d&2e**) were synthesized, and then added mercaptopropionic acid (MPA) to make the CdSe QDs water-soluble[40]. Cys_2-SpyCatcher proteins were recombinantly expressed, purified, and added to the mixture of CdS shell-formation precursors and water-soluble CdSe QDs, which were then gently heated at 90°C for 30 minutes. The resulting CdSe/CdS QD-SpyCatcher conjugates, with ~8 nm diameters, were purified and re-dispersed in PBS buffer. The organic-ligand-capped CdSe QDs displayed weak PL (Figure **2b**, black trace), while the SpyCatcher-conjugated CdSe/CdS QDs exhibited much stronger PL with a quantum yield (QY) of 35% (Figure **2b**, red trace). The enhanced PL emission can be attributed to CdS shell formation during the conjugation process. EDS spectra of the assembled core/shell QD-SpyCatcher conjugate chains revealed the presence of Cd and Se from the QD core, S from the QD shell, U from the uranyl acetate-stained curli amyloid fibrils, and Ni from the TEM grid (Figure **2c**, red trace).

COMMUNICATION

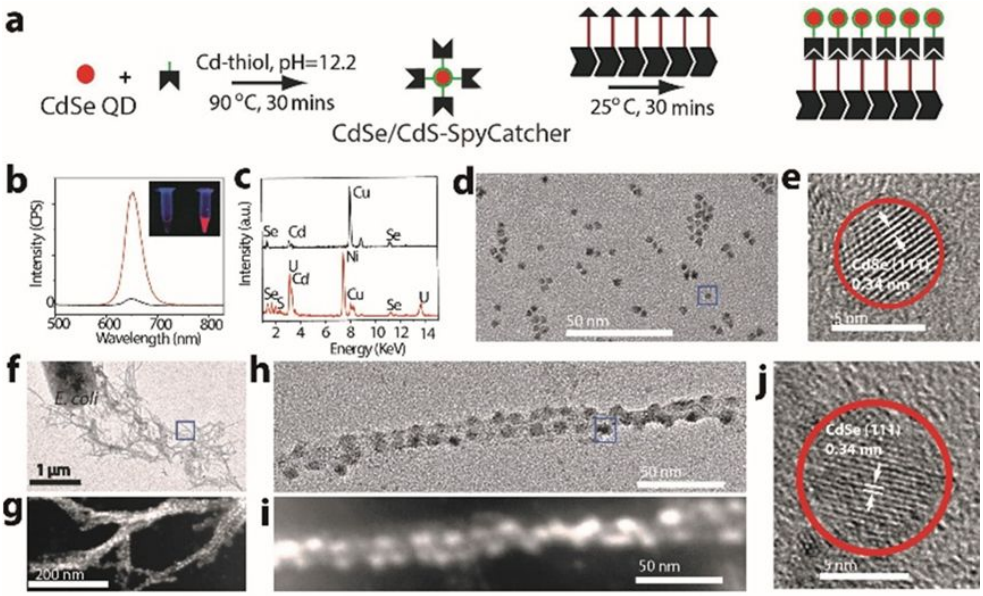

Fig. 2 Self-organization of CdSe/CdS QD-SpyCatcher conjugates with SpyTag-displaying amyloid curli fibrils synthesized by living cells. (**a**), Schematic illustration of the strategy for conjugating recombinant Cys_2-SpyCatcher to CdSe core QDs during shell synthesis and their assembly process. (**b**&**c**) PL emission and EDS spectra of the same concentration of starting CdSe QDs before conjugation (black curves) and the CdSe/CdS-SpyCatcher conjugates assembled with $CsgA_{SpyTag}$ amyloid fibrils with living cells (red curves). Inset photo in **b** shows CdSe QDs before conjugation (left) and the CdSe/CdS-SpyCatcher conjugates assembled with CsgASpyTag amyloid fibrils with living cells (right). (**d**&**e**) TEM and HRTEM images of the starting CdSe core QDs before conjugation. (**f**-**j**) TEM, HRTEM and STEM images of QD-SpyCatcher conjugates self-assembled on SpyTag-displaying amyloid curli fibrils with living cells, demonstrating that QDs are attached to the curli fibrils to form Jabuticaba-like nanostructures. The red circles in (**e**&**j**) indicate a single 6 nm CdSe QD and a single 8 nm CdSe/CdS core/shell QD-SpyCatcher conjugate assembled on amyloid fibrils, respectively. The amyloid fibrils are visualized by negative staining with uranyl acetate.

Large-scale self-organization of QDs is achieved by taking advantage of the high-fidelity coupling between SpyCatcher conjugated to CdSe/CdS QDs and SpyTag displayed on extracellular curli amyloid fibrils. To this end, we constructed *E. coli* that secreted $CsgA_{SpyTag}$, resulting in the formation of SpyTag-displaying curli amyloid fibrils. For the assembly of one-dimensional QD chains, CdSe/CdS QD-SpyCatcher conjugates were incubated with SpyTag-encoded fibrils in PBS at room temperature for 30 minutes to allow for complete SpyTag-SpyCatcher coupling. As depicted in Figure **2f-2j**, low-magnification TEM, HRTEM, and STEM images show 8 nm CdSe/CdS QD-SpyCatcher conjugates decorated the SpyTag-displaying amyloid fibrils.

Our synthesis strategy for QD-SpyCatcher conjugates is versatile and generalizable to QDs with variable compositions and surface ligands. We synthesized 5 nm red CdTe/CdS QD-SpyCatcher (650 nm, PL QY of 67%), 3 nm green CdTe/CdS QD-PilinC (530 nm, PL QY of 30%), and 4 nm blue ZnCdSe/ZnS QD-PilinN (440 nm, PL QY of 32%) conjugates as shown in Figures **3a, 3b, S1**. For example, red CdTe/CdS QDs with a PL emission peak at 630 nm were synthesized and then Cd-MPA was added [30]. Subsequently, Cys_2-SpyCatcher proteins were added and gently heated at 90°C for 30 minutes. The resulting CdTe/CdS QD-SpyCatcher conjugates had red PL emission at 650 nm and were stable in PBS buffer. We attribute the red shift of the PL emission peak of CdTe/CdS QDs during the shell growth process to a transition from type-I to type-II QDs during the gradual growth of the CdS shell [30,31]. We achieved highly specific organization of red CdTe/CdS QD-SpyCatcher conjugates with the corresponding SpyTag-displaying amyloid curli fibrils produced by living cells at large scales (20 cm^2, Figure **3c**). These red CdTe/CdS QD-SpyCatcher conjugates did not assemble with cell communities expressing the wild-type or the IsopeptagC-displaying amyloid fibrils, as shown in Figure **S2a**.

This platform for the multiplexed and scalable organization of protein-conjugated nanomaterials enables the creation of fluorescent multi-component bacteria-QD displays. We demonstrated this by first growing three different *E. coli* strains in patterns defined by stencil templates. These bacteria produced curli fibrils displaying SpyTag, IsopeptagC, or IsopeptagN, respectively. We compared the secretion efficiency of amyloid fibers with the spytag, isopeptagN and IsopeptagC linkages, respectively, and found that different peptide linkages have no visible impact the secretion efficiency of amyloid fibers. We then exposed the resulting cellular communities to mixed solutions containing red CdTe/CdS QD-SpyCatcher, green CdTe/CdS QD-PilinC, and blue ZnCdSe/ZnS QD-PilinN conjugates.

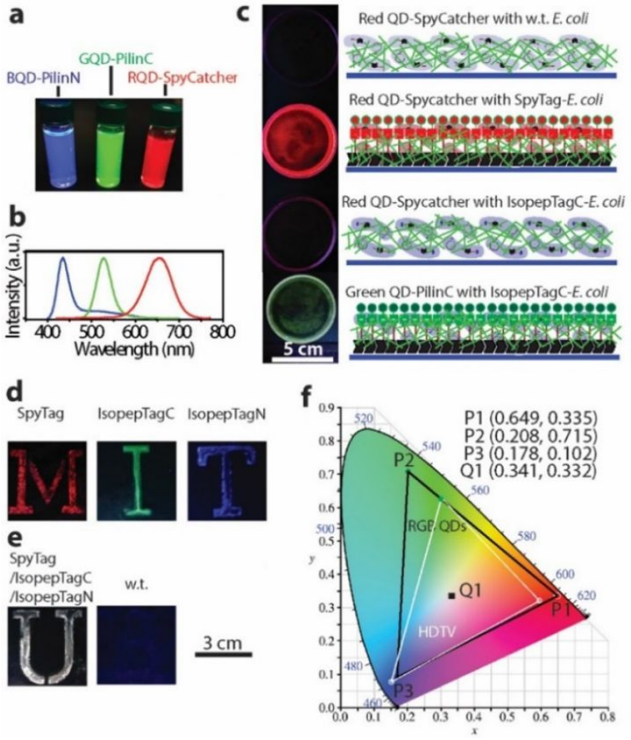

Fig. 3 Self-organization of RGB QD conjugates with living biofilms into full color displays. (**a**, **b**) Pictures and PL emission spectra of the red CdTe/CdS QD-SpyCatcher (RQD-SpyCatcher), green CdTe/CdS QD-PilinC (GQD-PilinC), and blue ZnCdSe/ZnS QD-PilinN (BQD-PilinN) conjugates. (**c**) Photographs and schematics of RQD-SpyCatcher conjugates assembled with *E. coli* expressing wild-type (wt) CsgA, $CsgA_{SpyTag}$, or $CsgA_{IsopeptagC}$ amyloid fibrils as well as GQD-PilinC conjugates self-assembled with $CsgA_{IsopeptagC}$ amyloid fibrils. (**d, e**) Photographs of mixed RQD-SpyCatcher, GQD-PilinC, BQD-PilinN conjugates self-assembled with $CsgA_{SpyTag}$ (Letter "M" as P1), $CsgA_{IsopeptagC}$ (Letter "I" as P2), $CsgA_{IsopeptagN}$ (Letter "T" as P3), $CsgA_{SpyTag}$ + $CsgA_{IsopeptagC}$ + $CsgA_{IsopeptagN}$ (Letter "U" as Q1), and $CsgA_{wt}$ (Letter "B") amyloid fibrils expressed by living cells grown with stencil templates. (**f**) Diagram of the CIE 1931 color space that shows the color properties of the RGB bacterial-QD patterns (P1, P2, P3 & Q1 in the black triangle and the location of the primary colours). The HDTV (Rec. 709) color space standard is plotted as a white triangle for comparison.

From these QD mixtures, *E. coli* expressing SpyTag-displaying curli fibrils specifically organized the red QD-SpyCatcher conjugates into a red "M" (Figure **3d**). *E. coli* expressing IsopeptagC-presenting curli fibrils specifically patterned the green QD-PilinC conjugates into a green "I". *E. coli* expressing IsopeptagN-displaying curli fibrils specifically organized blue QD-PilinN conjugates into a blue "T". When three different *E. coli* strains expressing SpyTag-, IsopeptagC-, and IsopeptagN-displaying curli fibrils were grown together, the multi-strain bacterial community captured the red, green, and blue QDs together, resulting in a white "U" (Figure **3e**). Thus, the resulting colors were determined by the identities and relative compositions of the cellular communities manufacturing various curli amyloid scaffolds. When wild-type *E. coli* was used, little QD fluorescence could be observed, as shown in Figure **3e**.

Figure **3f** shows the Commission Internationale de l'Eclairage (CIE) chromaticity coordinates of the red (0.649, 0.335), green (0.208, 0.715), and blue (0.178, 0.102) QD-protein conjugates with the living cell communities in the CIE 1931 chromaticity diagram. A high-definition television (HDTV) standard (Rec. 709) for red (0.64, 0.33), green (0.30, 0.60), blue (0.15, 0.06) is plotted for comparison. Our protein-conjugated QDs can achieve a larger (130%) gamut than that of the HDTV standard, especially in the green and red region, and can be selectively organized based on the composition of living cell populations.

We further confirmed the ability of the bacterial platform to assemble multi-component materials at the nanoscale. As depicted in Figure **4**, low-magnification TEM and HRTEM images showed 5 nm CdTe/CdS QD-SpyCatcher nanoparticles organized on SpyCatcher-displaying amyloid fibrils. HRTEM of a single chain with well-resolved lattice structures of CdTe confirmed the successful formation of QD chain structures. We found that self-organization only occurred in the presence of the SpyTag-SpyCatcher interactions, and that wild-type and IsopeptagC-displaying amyloid fibrils made by living cells did not bind significantly to red QD-SpyCatcher conjugates (Figure **3c**). However, cells that synthesized IsopeptagC-displaying amyloid fibrils did bind to 3 nm green CdTe/CdS QD-PilinC conjugates (Figure **3c**), thus demonstrating the specificity of the two orthogonal peptide-protein binding systems. Similarly, we also synthesized 4 nm ZnCdSe/ZnS QD-PilinN conjugates, which were able to self-assemble with living cell communities that produced IsopeptagN-displaying amyloid fibrils.

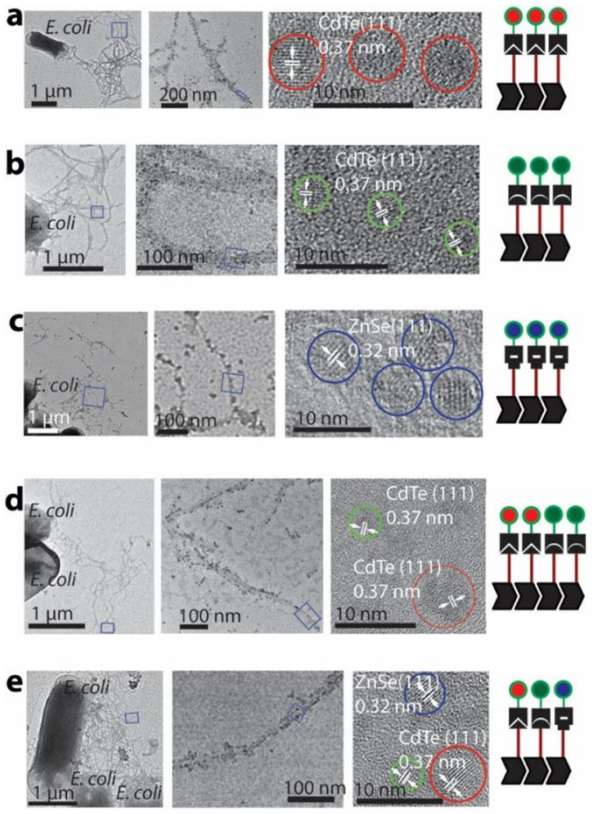

Fig. 4 TEM and HRTEM characterizations of the RGB QD-protein conjugates organized on amyloid fibrils with biofilms to form Jabuticaba-like nanostructures. (**a-c**) TEM, HRTEM images and schematics of the red CdTe/CdS QD-SpyCatcher conjugates self-assembled on $CsgA_{SpyTag}$, green CdTe/CdS QD-PilinC conjugates self-assembled on $CsgA_{IsopepTagC}$, and blue ZnCdS/ZnS QD-PilinN conjugates self-assembled on $CsgA_{IsopepTagN}$ displaying amyloid fibrils with living cells. (**d&e**) TEM, HRTEM images and schematics of red-emission

CdTe/CdS QD-SpyCatcher conjugates co-self-assembled with green-emission CdTe/CdS QD-PilinC, or blue-emission ZnCdSe/ZnS QD-PilinN on mixed $CsgA_{SpyTag}$, $CsgA_{IsopepTagC}$ subunits, or $CsgA_{IsopepTagN}$ displaying amyloid fibrils with living cells.

To explore the robustness of the abiotic-biotic materials platform, we grew and freeze-dried cells and their SpyTag-displaying amyloid fibrils, both in the absence and the presence of QD-SpyCatcher conjugates as shown in Figures **S2**&**S3**. In the absence of QD conjugates, the freeze-dried materials showed no PL. When we reconstituted these freeze-dried SpyTag-displaying amyloid fibrils in PBS, we found that they could specifically bind to QD-SpyCatcher conjugates. When the cells and amyloid fibrils were combined with green or red CdTe/CdS QD-SpyCatcher conjugates and then freeze-dried, the resulting self-assemblies exhibited stable and strong PL. Although freeze drying may damage cells, these effects should not degrade the protein-based materials as the cognate interactions between the protein-peptide partners used here are covalent [37, 38].

Our strategy enables the simultaneous organization of multiple functionalized QDs at the nanoscale. This approach was used to construct semiconductor-semiconductor heterostructures through specific and covalent SpyTag-SpyCatcher, IsopeptagN-PilinN, and IsopeptagC-PilinC binding interactions. We co-organized red-emission CdTe/CdS QD-SpyCatcher conjugates and green-emission CdTe/CdS QD-PilinC conjugates on composite amyloid fibrils consisting of $CsgA_{SpyTag}$ and $CsgA_{IsopeptagC}$ secreted by living cells (Figure **4d**). We also co-organized red-emission CdTe/CdS QD-SpyCatcher, green-emission CdTe/CdS QD-PilinC, and blue-emission ZnCdSe/ZnS QD-PilinN conjugates on composite amyloid fibrils consisting of $CsgA_{SpyTag}$, $CsgA_{IsopeptagC}$, and $CsgA_{IsopeptagN}$ (Figure **4e**). As shown in Figure S4a, the green emission is decreased while the red emission is increased, which could be potentially attributed to the existence of the Fluorescence Resonance Energy Transfer (FRET) after co-organization.[41] As shown in Figure S4b, we found the decreases in high-energy blue emission and concurrent increases in low-energy green and red emission in these heterostructures, which also could be attributed to FRET from the larger bandgap QDs to the smaller bandgap QDs. The above results indicated that our strategy to multiplex and orthogonal self-assembly of protein conjugated QDs with engineered biofilms would control the ratios of QDs that significantly impact the final Jabuticaba-like nanostructures and their optical properties.

In summary, we have demonstrted that mixed consortia of genetically engineered living cells can mediate the scalable and multiplexed self-organization of protein-conjugated QDs into full color Jabuticaba-like nanostructures. Isopeptide-bond-forming proteins conjugated to QDs and cognate binding tags displayed on curli amyloid fibrils were used to achieve specific SpyTag-SpyCatcher, IsopeptagN-PilinN, and IsopeptagC-PilinC interactions. The development of additional protein-peptide pairs would enable complex mixtures of protein-barcoded QDs to be programmably assembled on peptide-displaying biological scaffolds. Engineered amyloid fibrils and genetically encoded chemistries enabled the organization of large-scale RGB bacteria-QD displays. Although the demonstrations shown here are proof-of-principle experiments, we believe that they illustrate the utility of bacterial communities for multiplexed assembly of inorganic nanomaterials. This work is complementary to previous work demonstrating that spatiotemporal control of amyloid expression by living *E. coli* enables patterning of materials across multiple length scales[29]. Future improvements may include controlling the synthesis of genetically engineered amyloid fibrils with synthetic gene circuits [42, 43] to implement autonomous cell-based biofabrication platforms, as well as integrating protein design [44, 45] to achieve finer control of nanoscale structures. Ultimately, we envision that this work will facilitate the patterning of multi-functional nanomaterials for large-area devices using scalable, low-cost, and renewable architectures.

Conflicts of interest

There are no conflicts to declare.

Acknowledgements

We thank M. Howarth (Oxford University) for the SpyTag-SpyCatcher, IsopeptagC-PilinC, and IsopeptagN-PilinN constructs. The use of facilities within the Institute for soldier Nanotechnologies (ISN) and Center for Materials Science and Engineering (CMSE) at MIT is acknowledged. This work was supported by the Office of Naval Research and Army Research Office. This work was also supported in part by the MRSEC Program of the National Science Foundation under award number DMR-0819762. Z.D. acknowledges support from the MIT RLE Translational Fellows program, Natural Science Foundation of China (22075129). A.Y.C. acknowledges support from the Hertz Foundation, the Department of Defense, and NIH Medical Scientist Training Program grant T32GM007753. T.K.L. acknowledges support from the Presidential Early Career Award for Scientists and Engineers and the NIH New Innovator Award (1DP2OD008435).

Notes and references

1 T.-C. Tang, B. An, Y. Huang, S. Vasikaran, Y. Wang, X. Jiang, T. K. Lu and C. Zhong, *Nature Reviews Materials*, 2020, **6**, 332-350.
2 B. Z. Tian, J. Liu, T. Dvir, L. H. Jin, J. H. Tsui, Q. Qing, Z. G. Suo, R. Langer, D. S. Kohane and C. M. Lieber, *Nat Mater*, 2012, **11**, 986-994.
3 J. P. Giraldo, M. P. Landry, S. M. Faltermeier, T. P. McNicholas, N. M. Iverson, A. A. Boghossian, N. F. Reuel, A. J. Hilmer, F. Sen, J. A. Brew, et al., *Nat Mater*, 2014, **13**, 530-530.
4 M. S. Mannoor, Z. W. Jiang, T. James, Y. L. Kong, K. A. Malatesta, W. O. Soboyejo, N. Verma, D. H. Gracias and M. C. McAlpine, *Nano Lett*, 2013, **13**, 2634-2639.
5 X. Wang, J. Pu, B. An, Y. Li, Y. Shang, Z. Ning, Y. Liu, F. Ba, J. Zhang and C. Zhong, *Advanced Materials*, 2018, **30**, 1705968.
6 Y. Li, K. Li, X. Wang, M. Cui, P. Ge, J. Zhang, F. Qiu and C. Zhong, *Science Advances*, 2020, **6**, eaba1425.
7 X. Wang, J. Pu, Y. Liu, F. Ba, M. Cui, K. Li, Y. Xie, Y. Nie, Q. Mi, T. Li, et al., *National Science Review*, 2019, **6**, 929-943.

8 Q. Liu, K. Wan, Y. Shang, Z. G. Wang, Y. Zhang, L. Dai, C. Wang, H. Wang, X. Shi, D. Liu, et al., *Nat Mater*, 2021, **20**, 395-402.
9 L. Xu, S. R. Gutbrod, A. P. Bonifas, Y. Su, M. S. Sulkin, N. Lu, H.-J. Chung, K.-I. Jang, Z. Liu, M. Ying, et al., *Nature Communications*, 2014, **5**, 3329.
10 Q. Wang, H. Wang, C. Lin, J. Sharma, S. Zou and Y. Liu, *Chem Commun (Camb)*, 2010, **46**, 240-242.
11 G. M. Whitesides and B. Grzybowski, *Science*, 2002, **295**, 2418-2421.
12 S. G. Zhang, *Nat Biotechnol*, 2003, **21**, 1171-1178.
13 Y. Yang, Z. Wu, L. Wang, K. Zhou, K. Xia, Q. Xiong, L. Liu, Z. Zhang, E. R. Chapman, Y. Xiong, et al., *Nat Chem*, 2021, **13**, 335-342.
14 P. W. K. Rothemund, *Nature*, 2006, **440**, 297-302.
15 J. Sharma, R. Chhabra, A. Cheng, J. Brownell, Y. Liu and H. Yan, *Science*, 2009, **323**, 112-116.
16 S. Woo and P. W. K. Rothemund, *Nat Chem*, 2011, **3**, 620-627.
17 A. Kuzyk, R. Schreiber, Z. Y. Fan, G. Pardatscher, E. M. Roller, A. Hogele, F. C. Simmel, A. O. Govorov and T. Liedl, *Nature*, 2012, **483**, 311-314.
18 Y. G. Zhang, F. Lu, K. G. Yager, D. van der Lelie and O. Gang, *Nat Nanotechnol*, 2013, **8**, 865-872.
19 R. Schreiber, J. Do, E. M. Roller, T. Zhang, V. J. Schuller, P. C. Nickels, J. Feldmann and T. Liedl, *Nat Nanotechnol*, 2014, **9**, 74-78.
20 S. M. Douglas, I. Bachelet and G. M. Church, *Science*, 2012, **335**, 831-834.
21 J. D. Hartgerink, E. Beniash and S. I. Stupp, *Science*, 2001, **294**, 1684-1688.
22 S. W. Lee, C. B. Mao, C. E. Flynn and A. M. Belcher, *Science*, 2002, **296**, 892-895.
23 C. B. Mao, D. J. Solis, B. D. Reiss, S. T. Kottmann, R. Y. Sweeney, A. Hayhurst, G. Georgiou, B. Iverson and A. M. Belcher, *Science*, 2004, **303**, 213-217.
24 C. L. Chen and N. L. Rosi, *Angew Chem Int Edit*, 2010, **49**, 1924-1942.
25 X. N. Dang, H. J. Yi, M. H. Ham, J. F. Qi, D. S. Yun, R. Ladewski, M. S. Strano, P. T. Hammond and A. M. Belcher, *Nat Nanotechnol*, 2011, **6**, 377-384.
26 B. Ding, Z. Deng, H. Yan, S. Cabrini, R. N. Zuckermann and J. Bokor, *J Am Chem Soc*, 2010, **132**, 3248-3249.
27 X. Lan, X. Lu, C. Shen, Y. Ke, W. Ni and Q. Wang, *Journal of the American Chemical Society*, 2015, **137**, 457-462.
28 A. Y. Chen, Z. T. Deng, A. N. Billings, U. O. S. Seker, M. Y. Lu, R. J. Citorik, B. Zakeri and T. K. Lu, *Nat Mater*, 2014, **13**, 515-523.
29 P. Q. Nguyen, Z. Botyanszki, P. K. R. Tay and N. S. Joshi, *Nat Commun*, 2014, **5**.
30 M. Källberg, H. Wang, S. Wang, J. Peng, Z. Wang, H. Lu and J. Xu, *Nat Protoc*, 2012, **7**, 1511-1522.
31 J. J. Dong, C. E. Castro, M. C. Boyce, M. J. Lang and S. Lindquist, *Nat Struct Mol Biol*, 2010, **17**, 1422-U1449.
32 T. P. J. Knowles and M. J. Buehler, *Nat Nanotechnol*, 2011, **6**, 469-479.
33 T. Scheibel, R. Parthasarathy, G. Sawicki, X. M. Lin, H. Jaeger and S. L. Lindquist, *P Natl Acad Sci USA*, 2003, **100**, 4527-4532.
34 C. Zhong, T. Gurry, A. A. Cheng, J. Downey, Z. T. Deng, C. M. Stultz and T. K. Lu, *Nat Nanotechnol*, 2014, **9**, 858-866.
35 M. R. Chapman, L. S. Robinson, J. S. Pinkner, R. Roth, J. Heuser, M. Hammar, S. Normark and S. J. Hultgren, *Science*, 2002, **295**, 851-855.
36 J. F. Smith, T. P. J. Knowles, C. M. Dobson, C. E. MacPhee and M. E. Welland, *P Natl Acad Sci USA*, 2006, **103**, 15806-15811.
37 B. Zakeri, J. O. Fierer, E. Celik, E. C. Chittock, U. Schwarz-Linek, V. T. Moy and M. Howarth, *P Natl Acad Sci USA*, 2012, **109**, E690-E697.
38 B. Zakeri and M. Howarth, *J Am Chem Soc*, 2010, **132**, 4526-+.
39 Z. T. Deng, A. Samanta, J. Nangreave, H. Yan and Y. Liu, *J Am Chem Soc*, 2012, **134**, 17424-17427.
40 Z. T. Deng, O. Schulz, S. Lin, B. Q. Ding, X. W. Liu, X. X. Wei, R. Ros, H. Yan and Y. Liu, *J Am Chem Soc*, 2010, **132**, 5592-+.
41 K. E. Sapsford, L. Berti and I. L. Medintz, *Minerva Biotecnol*, 2004, **16**, 247-273.
42 S. Payne, B. C. Li, Y. X. L. Cao, D. Schaeffer, M. D. Ryser and L. C. You, *Mol Syst Biol*, 2013, **9**.
43 R. J. Gubeli, K. Burger and W. Weber, *Biotechnol Adv*, 2013, **31**, 68-78.
44 N. P. King, W. Sheffler, M. R. Sawaya, B. S. Vollmar, J. P. Sumida, I. Andre, T. Gonen, T. O. Yeates and D. Baker, *Science*, 2012, **336**, 1171-1174.
45 J. M. Fletcher, R. L. Harniman, F. R. H. Barnes, A. L. Boyle, A. Collins, J. Mantell, T. H. Sharp, M. Antognozzi, P. J. Booth, N. Linden, et al., *Science*, 2013, **340**, 595-599.